Talanta 235 (2021) 122817

Contents lists available at ScienceDirect

Talanta

journal homepage: www.elsevier.com/locate/talanta

Lipid response of hepatocellular carcinoma cells to anticancer drug detected on nanostructure-assisted LDI-MS platform

Tao Wang [a], Xingyue Liu [a], Xuetong Qu [a], Yuexin Li [a], Xiao Liang [b,**], Jianmin Wu [a,*]

[a] Institution of Analytical Chemistry, Department of Chemistry, Zhejiang University, Hangzhou, 310058, China
[b] Department of General Surgery, Sir Run Run Shaw Hospital, School of Medicine, Zhejiang University, Hangzhou, 310016, China

ARTICLE INFO

Keywords:
Nanostructure-assisted laser desorption/ionization mass spectrometry (NALDI-MS)
Hepatocellular carcinoma cell
Drug susceptibility
Lipidomics

ABSTRACT

High heterogeneity of hepatocellular carcinoma (HCC) tumor has become an obstacle to select effective therapy for the treatment of HCC patients. Methods that can guide the decision on therapy choice for HCC treatment are highly demanded. Evaluating the drug response of heterogeneous tumor cells at the molecular level can help to reveal the toxicity mechanism of anticancer drugs and provide more information than current cell-based chemosensitivity assays. In the present work, nanostructure-assisted laser desorption/ionization mass spectrometry (NALDI-MS) was used to investigate the lipid response of HCC cells to anticancer drugs. Three types of HCC cells (LM3, Hep G2, Huh7) were treated with sorafenib, doxorubicin hydro-chloride, and cisplatin. We found that the lipid profiles of HCC cells changed a lot after the drug treatment, and the degree of lipid changes was related to the cell viability. Two pairs of fatty acids C16:1/C16:0 and C18:1/C18:0 were found to be strongly related to the viability of HCC cells after drug treatment, and were more sensitive than Methyl-thiazolyl tetrazolium (MTT) assay. Accordingly, they can act as sensitive and comprehensive indexes to evaluate the drug susceptibility of HCC cells. In addition, the peak ratio of several neighboring phospholipids displayed high correlation with drug response of specific cell subtype to specific drug. The ratio of neighboring lipids may be traced back to the activity of enzyme and gene expression which regulate the lipidomic pathway. This method provides drug response of heterogenous tumor cells at molecular level and could be a potential candidate to precise tumor chemosensitivity assay.

1. Introduction

Hepatocellular carcinoma (HCC) accounts for nearly 90% of primary liver cancer and ranks as the third leading cause of cancer death with poor prognosis. Although there are developed chemotherapy and targeted drugs for HCC patients, the median survival of patients with advanced HCC is still less than 20 months [1]. The high tumor heterogeneity of HCC has become an obstacle to efficient chemotherapy and targeted medical treatment of HCC patients [2,3]. Heterogeneous HCC cells show different sensitivity and resistance to anticancer drugs, leading to gaps in the effectiveness of chemotherapy in patients [4,5]. The combination of clinical, pathological, and gene expression data may help in the prediction of HCC prognosis. For examples, several genes (TP53, CTNNB1, etc.) [6–8] and proteins (VEGF, SDF-1, etc.) [9,10] have been proposed as potential drug targets for HCC. Their mutation or expression level could guide the medical decision for the treatment of HCC patients [11]. However, the sensitivity and specificity of these biomarkers to HCC patients remain to be improved, and more multi-omics biomarkers related to the prognosis of HCC are needed to be explored to improve the medical effect of HCC patients. Metabolome is at the downstream of genome and proteome. It provides biological terminal information and can better reflect the phenotypic changes, physiological and pathological conditions of individuals [12]. Therefore, studying the susceptibility and cellular metabolites changes of heterogeneous HCC cells to different anticancer drugs will provide key information for patients' precise medication.

Tumor chemosensitivity assay in vitro is an important method to guide individualized medication for HCC patients in the clinic [13]. Methyl-thiazolyl tetrazolium (MTT) assay [14] and adenosine triphosphate (ATP) assay [15] are the most commonly used strategies to evaluate the cellular chemosensitivity to anticancer drugs. Flow cytometry with fluorescent staining kits is also employed to detect the effects of

* Corresponding author. Wu Institution of Analytical Chemistry, Department of Chemistry, Zhejiang University Hangzhou, 310058, China.
** Corresponding author. Department of General Surgery, Sir Run Run Shaw Hospital, School of Medicine, Zhejiang University, Hangzhou, 310016, China.
E-mail addresses: srrshlx@zju.edu.cn (X. Liang), wjm-st1@zju.edu.cn (J. Wu).

https://doi.org/10.1016/j.talanta.2021.122817
Received 17 July 2021; Received in revised form 18 August 2021; Accepted 19 August 2021
Available online 20 August 2021

drugs on the cell cycle and cell apoptosis [16]. However, these methods either work best for detecting the later stages of apoptosis when the metabolic activity of the cells is severely reduced or provide limited cellular information due to the limited diversity of fluorescently labeled molecules [17]. Researches on the early detection of cell death during drug treatment and identification of drug-sensitive/resistant biomarkers are required to screen new drugs or drug targets, monitor the progress of drug response, and formulate personalized medication plans for patients [18]. Taking into account of the high heterogeneity of HCC cells, the recognition of HCC cell subtypes must be achieved before the drug susceptibility test. In our previous work, a panel of cell peptides and lipids detected by mass spectrometry have been successfully used to discriminate 5 subtypes of HCC cell lines [19,20].

Mass spectrometry (MS) technologies are powerful platforms for lipid profiling due to their high sensitivity and molecular identification capability. Several works on the in-depth study of metabolic changes related to drug response of cancer cells have been achieved on liquid chromatography (LC) MS and gas chromatography (GC) MS platforms [21–23]. However, for clinical application, high-throughput and high-speed mass spectrometry technology is highly demanded. Without any chromatographic separation, matrix-assisted laser desorption/ionization (MALDI) MS has become a promising platform to analyze complex biofluid samples in the clinic owing to its high throughput and high-speed merits [24]. The emergence of matrix-free LDI technologies [25–29] further pushes forward the application of these platforms in metabolomics research, since the interference of organic matrix fragments and uneven co-crystallization of the organic matrix were avoided [30]. We previously reported that a NALDI-chip patterned with silicon nanowire array can effectively detect cell lipids in a high-throughput way, and the discrimination of HCC cell subtypes was also achieved on this platform [20].

In the present work, we studied the lipid profile changes of three subtypes of HCC cells after the treatment of different anticancer drugs by NALDI-MS technology. We found that the peak ratio change of several types of lipids was associated with the type and dose of anticancer drugs, while some types of lipid molecules related to the cell subtype were highly conserved. Two pairs of fatty acids C16:1/C16:0 and C18:/C18:0 were found to be strongly related to the death degree of HCC cells after drug treatment, and their ratio values could act as indexes to evaluate cell viability that were more sensitive than MTT assay. The peak ratios of lipids are simple and effective indicators because they don't need additional internal standards and can effectively solve the absolute quantitative problem encountered in LDI-MS detection. In addition, drug susceptibility of heterogeneous HCC cell lines could be revealed by the ratio of neighboring lipids who sharing the similar molecular structures but different degree of unsaturation, which may be traced back to the activity of enzyme and gene expression regulating the lipidomic pathway, such as stearoyl-CoA desaturase 1 (SCD1). This MS-based drug susceptibility test could be a new platform for tumor chemosensitivity assay and the discovery of drug targets for heterogeneous tumor cells, which may ultimately lead to the development of personalized cancer treatment.

2. Experimental

2.1. Chemicals and materials

Silicon wafers (n-type, (1–10 Ω cm), <100>) were purchased from Lijing Silicon Materials Corp. (Quzhou, China). AZ4620 was obtained from AZ Electronic Materials (Japan). Lauric acid (C12:0), palmitic acid (C16:0), stearic acid (C18:0), arachidic acid (C20:0), teracosanoic acid (C24:0), 1, 2-dipalmitoyl-sn-glycero-3-phosphoethanolamine (DPPE 16:0/16:0) and 1, 2-dioleoyl-sn-glycero-3-phosphate (LPG 14:0) were purchased from Aladdin Co. (Shanghai, China). A-cyano-4-hydroxycinnamic acid (CHCA) and 2, 5-dihydroxybenzoic acid (DHB) were purchased form Bruker Daltonics Inc. (Billerica, USA). Methylthiazolyl tetrazolium (MTT) and Dulbecco's modified Eagle's medium (DMEM), trypsin-EDTA and antibiotics, fetal bovine serum (FBS) were purchased from Sigma-Aldrich (Saint Louis, MO,U. S. A.), Gibco Corp. (Grand Island, NY, USA) and Biological Industries Corp. (Israel), respectively. HCCLM3 (LM3), and Huh7 cells were obtained from the Cell Bank of the Chinese Academy of Science (Shanghai, China). Hep G2 cells were obtained from the American Tissue Culture Collection (ATCC). (Shanghai, China). Sorafenib, doxorubicin hydro-chloride, and cisplatin were purchased from Santa Cruz Biotechnology (Dallas, U.S.A.) and Shanghaiyuanye Bio-Technology Co. (Shanghai, China), respectively. All other reagents used in this experiment were of analytical reagent grade or HPLC grade.

2.2. Fabrication of the Si-NALDI target

The preparation of Si-NALDI target was the same as previously reported [20] with the addition of hydrophobic modification steps. Briefly, a silicon wafer (n type, 1–10 Ω/cm, <100>) was cut into pieces with the size of 5.5 cm × 2.5 cm and thoroughly cleaned by several kinds of solutions in the following order: isopropyl alcohol, distilled (DI) water, piranha solution (H_2SO_4: H_2O_2 = 7 : 3), isopropyl alcohol and DI water. After the cleaning procedure was completed, the silicon wafer was dried and immersed in a toluene solution containing 1.7 mol L^{-1} *N*-octadecyltrichlorosilane (OTS, Sigma-Aldrich, Saint Louis, MO, U. S. A.) for 60 min. Once the reaction finished, the silicon wafer was transferred into fresh toluene and sonicated to remove the physically adsorbed reactants. The dried OTS modified silicon wafer was spin-coated with an AZ4620 photoresist and pre-baked at 95 °C for 3 min. Then the wafer was covered by a designed photomask with a spot array (4 × 11 spots, the diameter of spots was 3 mm with a spacing distance of 1.5 mm, location IDs were placed on the north side and west side) and exposed to UV light for 60 s. The exposed photoresist was eluted by an aqueous solution of 0.7% NaOH. After washed with DI water and dried under a dry nitrogen stream, a post-bake procedure was performed at 115 °C for 10 min to facilitate the corporation between photoresist film and surface of silicon slice. Silicon nanowires array (Si NWs) were prepared via the one-step metal-assisted chemical etching (MACE) method. The patterned silicon wafer was immersed into an etching solution containing 4.8 M HF and 0.02 M $AgNO_3$ for 15 min (caution: HF is highly toxic and contact with the skin should be avoided), and then washed by DI water for three times to remove the residual hydrofluoric acid. Diluted HNO_3 (1:1) was added and submerged the silicon wafer for 30 min to dissolve the silver on the nanowire surface. Finally, acetone was used to remove the residual photoresist on the silicon wafer. Thus a Si-NALDI target with an array of 4 × 11 identical Si NWs spots was prepared.

2.3. Characterization

Scanning electron microscope (SEM) images were performed on HITACHI SU8010 field emission SEM and the primary electron voltage was 3 kV. The contact angle was measured on a contact angle measuring instrument (POWEREACH®, JC2000D1).

2.4. Cell culture

Cells (LM3, HepG2, Huh7) were grown in Dulbecco's modified Eagle's medium (DMEM) with 10% fetal bovine serum (FBS) and 0.1% antibiotics (100 U mL^{-1} penicillin and 100 μg mL^{-1} streptomycin). Cells were kept in an incubator at 37 °C with 5% CO_2 and subcultured at 80%–85% confluence.

2.5. MTT cell viability assay and ATP cell viability assay

MTT assay: Cells were seeded into 96-well plates at a density of 10,000 cells per well, and incubated for 24 h. After that, each well was

gently washed with PBS solution for three times, and then cells were treated with different concentrations of sorafenib, doxorubicin hydrochloride (DOX), and cisplatin (CDDP) for 24 h and 48 h, respectively. The drug concentrations were listed in Table 1, and each drug concentration has 5 replicated wells. For MTT assay, culture media were replaced by MTT reagent (0.5 mg mL^{-1}) then incubated for 4 h. All solutions in the wells were discarded and dimethyl sulfoxide (DMSO) was used for re-dissolving. The absorbance at 570 nm was measured by a microplate reader.

ATP assay: The sensitive "firefly'' reaction is used in the ATP assay to determine the level of cellular ATP, and ATP content is directly proportional to the cell number. Cells were seeded, grown, and treated with drugs as described in the MTT cell viability assay. The CellTiter-Lumi™ Plus (Beyotime Biotechnology, Shanghai, China) was used for the luminometric measurement of cell viability. White 96-well plates were used in ATP assay to reduce the fluorescence interference between the wells. ATP standards were diluted according to the manufacturer's standard protocol and added to each well after drug treatment. After 30 min's incubation, the plates were measured using an Infinite F 50 absorbance reader (Tecan Austria GmbH, Austria).

2.6. Harvesting cells after drug treatment

Cells were seeded into 6-well plates with a density of 2×10^5 cells per well and incubated overnight. Drugs with different concentrations (Table 1) were added into wells and incubated with cells for 24 h, respectively. Each concentration of the drug was replicated for three times. After drug treatment, cells were collected after trypsin treatment and then washed with PBS for three times. Finally, the cells were resuspended in PBS at a concentration of 5×10^6 cells mL^{-1}. All collected cell samples were stored in a −80 °C refrigerator before use.

2.7. Lipid extraction and sample preparation

Lipids of cells were extracted using the Folch method [31] with minor modification. 20 μL cell sample was added into an extractive solution containing 30 μL DI water, 100 μL methanol and 200 μL dichloromethane, and then vortexed for 5 min. Centrifugation was performed at ~2500 g for 5 min to isolate the bottom layer. The organic phase containing extracted lipids was dried by a nitrogen stream and re-dissolved with 30 μL methanol. 2 μL of the extracted lipids was dropped on a sample spot of the Si-NALDI target and dried.

2.8. NALDI-MS analysis of cell lipids

An UltrafeXtreme MALDI-TOF/TOF instrument (Bruker Daltonics Corp.) equipped with a 355 nm Nd: YAG laser beam was used for NALDI-MS analysis. The Si-NALDI target with the dried sample was fixed onto a custom made plate designed to match with the MALDI-TOF-MS instrument. Mass spectra in both negative ion mode (m/z 200–1000) and positive ion mode (m/z 700–1000) were acquired. The laser pulse energy was set to 16 μJ with a laser focus diameter around 100 μm. Ions were resulted from 120 ns pulsed ion extraction and 2.7 kV acceleration voltage. A mixture sample of C12:0, C16:0, C18:0, C20:0, C24:0 and DPPE 32:0 was used for mass calibration in negative ion mode. A-cyano-4-hydroxycinnamic acid (CHCA) and peptide standards (Bruker Daltonics Corp.) were used for mass calibration in positive ion mode. 1500 laser shots were averaged for each mass spectrum. Information of lipid structures was obtained by the tandem mass spectrometry (MS/MS) analysis on the MALDI-TOF/TOF instrument. To find the most suitable laser energy for NALDI-MS detection, a solution containing 1 mM LPG (14:0) in methanol was used as a standard solution. The parent ion ($[M-H]^-$) peak intensity of LPG (14:0) and its survival yield were regarded as two important comparison parameters. The survival yield is calculated by the following equation: Survival yield $= I_{parent}/(I_{parent} + I_{product}) \times 100\%$. Measurement of lipids by LC-MS/MS in negative ion mode served as a supplement and confirmation of MALDI MS/MS detection. The experimental section of LC-MS/MS measurement was shown in the supporting information. LIPID MAPS® online tools (https://www.lipidmaps.org/) were used to match the information of parent ions with the corresponding MS/MS data.

Table 1
Concentration list of three kinds of anticancer drugs used in this research.

	Conc.1 (μmol L^{-1})	Conc.2 (μmol L^{-1})	Conc.3 (μmol L^{-1})	Conc.4 (μmol L^{-1})	Conc.5 (μmol L^{-1})
Sorafenib	0	0.31	0.63	1.25	2.50
DOX	0	2.5	5	10	20
CDDP	0	20	40	80	160

2.9. Statistical analysis

The originally obtained mass spectra were baseline subtracted in FlexAnalysis 3.4 (Bruker Daltonics Corp.) and then exported as ASCII files for statistical analysis. Two criteria were used to judge an ion peak that could be included in the following multivariate data analysis: (1) its signal-to-noise (S/N) ratio was greater than 5; (2) its frequency occurred in the mass spectra of the same sample was greater than 66%. All peaks of identified lipids in the mass spectrum were normalized with respect to the total ion current. Principal component analysis (PCA), linear discriminant analysis (LDA) and Spearman correlation coefficient analysis were performed on MATLAB (MathWorks, U. S. A.). SPSS Ver. 22 (IBM, Chicago, IL, USA) was used for the Pearson correlation coefficient analysis.

2.10. Western blotting

Total proteins of cells were extracted with the use of radio immunoprecipitation assay (RIPA) buffer (Beyotime Biotechnology, Shanghai, China) containing protease and phosphatase inhibitors. The amount of proteins was determined through bicinchoninic acid protein assay. Protein samples were separated by sodium dodecyl sulfate polyacrylamide gel electrophoresis (SDS-PAGE) and then transferred onto polyvinylidene fluoride (PVDF) membranes. Membranes were blocked with 5% non-fat milk in TBS-T for 2 h, and then were incubated with the SCD1-specific antibody for 4 h at room temperature. Secondary goat anti-mouse SCD1 antibody (Affinity Biosciences LTD.) was used at a dilution of 1:5000 with incubation for 1 h at room temperature. Signals were detected by chemiluminescent HRP substrate (Beyotime Biotechnology, Shanghai, China) and images were acquired using an electrochemiluminescence (ECL) detection system (Pierce).

3. Results and discussion

3.1. Lipid profiling and subtype discrimination of drug-treated HCC cells by NALDI-MS

In the present study, one multi-kinase inhibitor (sorafenib) and two chemotherapeutic agents (doxorubicin hydrochloride, cisplatin) which are commonly used in the treatment of HCC were employed as the model anticancer drugs, and the concentration of each drug used in this study was shown in Table 1. After treatment with a series concentration of sorafenib, doxorubicin hydrochloride (DOX) and cisplatin (CDDP) for 24 h, the lipid profiles of LM3, Hep G2 and Huh7 cells were acquired to explore whether the cellular lipid changes were related to the degree of cell viability and the drug type.

Lipids extracted from cells were analyzed in both positive and negative ion modes by NALDI-MS using a Si-NALDI target, and all the experimental procedures were shown in Fig. 1. Compared with the complex background interference of traditional MALDI matrix CHCA and DHB, there almost no background interference caused by the Si-

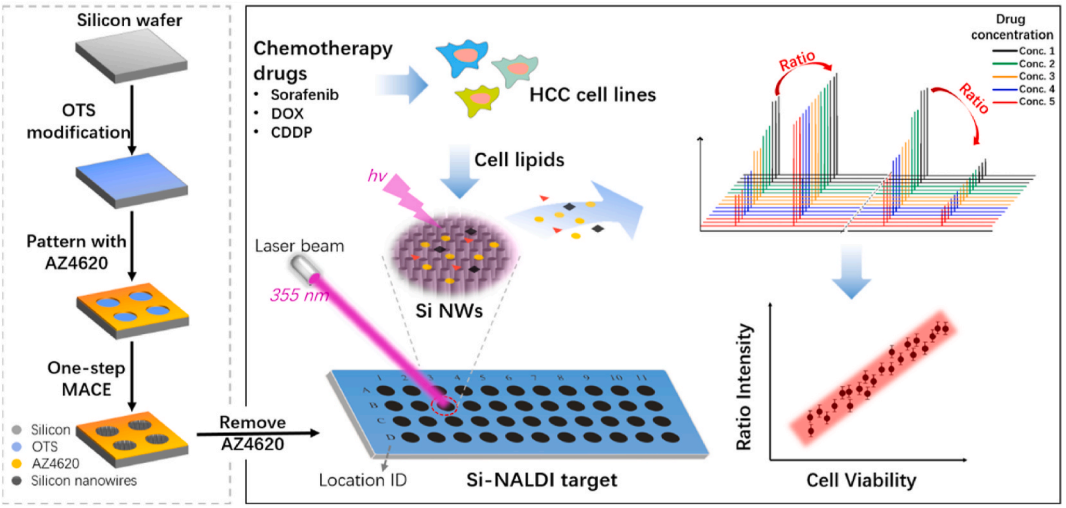

Fig. 1. Schematic diagram of the process of Si-NALDI target fabrication, lipid extraction, mass spectrometry detection and data analysis after the HCC cells were incubated with different anticancer drugs.

NALDI target at the *m/z* range of 200–1000 (Fig. S1). Our previous works have indicated that vertical silicon nanowires array (Si NWs) is an idea NALDI substrate for lipid analysis [20,32,33]. In this work, we developed a Si-NALDI target containing 4 × 11 hydrophilic Si NWs spots (diameter: 3 mm), which was surrounded by hydrophobic OTS (Fig. S2a and b). The hydrophobic nature of OTS transformed the un-etched Si surface from hydrophilic (contact angle: 63°) to hydro-phobic (contact angle: 108°) that can make each drop of sample solution confined with the patterned SiNWs array spots homogeneously (Fig. S2). The laser energy was set to 85% during the MS detection to maintain high ion survival yield and intensity of precursor ion at the same time (Fig. S3). According to the fatty acid fragments and phospholipid head of the precursor ion peaks detected in MS/MS analysis, the structure of the lipid molecules detected in NALDI-MS was matched through the MS/MS database of LIPIDMAPS® (Fig. S4, Table S1). The identified lipids were major seven species including fatty acids (FAs), phosphatidylethanolamines (PEs), phosphatidylinositols (PIs), phosphatidylserines (PSs), and phosphocholines (PCs) while several triacylglycerols (TAGs) and sphingolipids (SMs) were also identified. Affected by the high electronegative groups such as carboxyl group, hydroxyl group, phosphoric acid group and sulfonic acid group, lipids including FAs, PEs, PIs, PSs, PGs and PSs were detected under negative ion mode (Fig. 2a), and PCs were detected under positive ion mode due to their electropositive phosphorylcholine groups (Fig. 2b).

Lipid profiles of LM3, Hep G2 and Huh7 cells showed that showed that the proportion of these lipids in each cell line was slightly different (Fig. S5). MS spectra of each cell line treated with each drug concentration were acquired and averaged from 9 replicated detection. In the full lipid MS spectra, more than 130 peaks were identified (Table S1). After data pretreatment such as baseline subtraction and normalization, linear discriminated analysis (LDA, fisher) and principal component analysis (PCA) were conducted. The result of LDA indicated that the

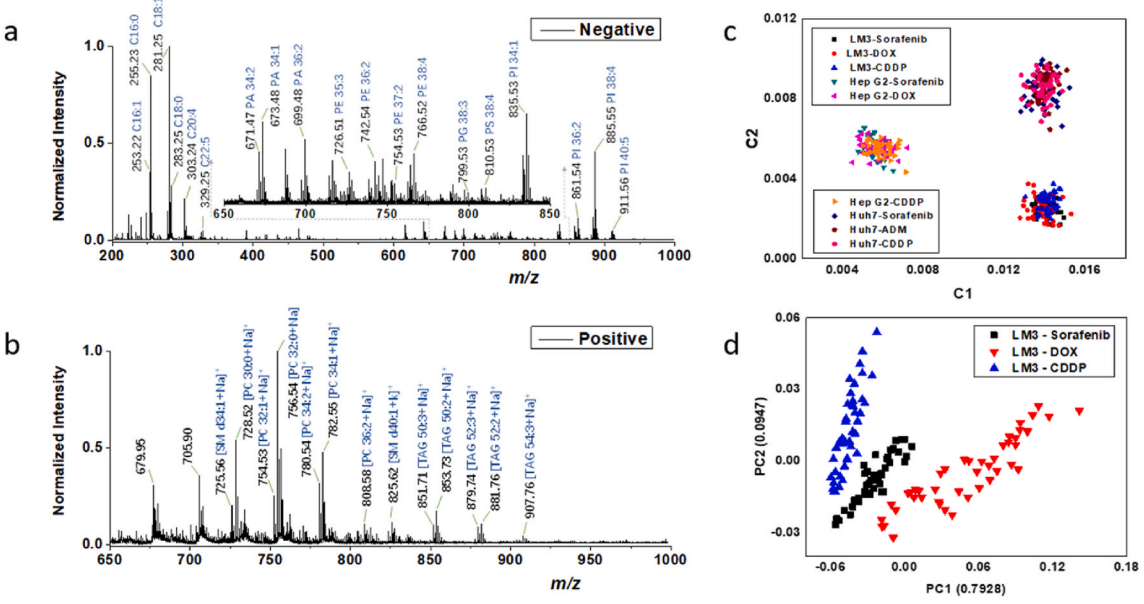

Fig. 2. Distributions of lipids in the mass spectrum detected in (a) negative ion mode and (b) positive ion mode. Both were detection result of LM3 cells without any drug treatment. (c) Linear discriminated analysis (LDA, fisher) result of LM3, Hep G2 and Huh7 cells that incubated with series concentration of sorafenib, DOX and CDDP for 24 h. (d) Principle component analysis (PCA) result of LM3 cells incubated with series concentration of sorafenib, DOX and CDDP for 24 h. The series concentration refers to the drug concentration listed in Table 1.

three HCC cell lines could be clearly discriminated without affecting by drug treatment (Fig. 2c) while the result of PCA showed that the lipid profile of the same cells changed with the treatment of different drugs (Fig. 2d). The loading plots of LDA/PCA were shown in Fig. S6. These results demonstrated that the full lipid profiles of HCC cells can not only distinguish cell subtypes but also reflect the drug response of a specific cell line to different types of anticancer drugs.

3.2. Chemosensitivity of HCC cells to different anticancer drugs measured by MTT and ATP assay

LM3, Hep G2 and Huh7 cells were harvested after treatment with a series concentration of anti-cancer drugs (Table 1) for 24 h. Among the three types of cells, LM3 is highly metastatic and showed a strong migration ability in the scratch experiment (Fig. S7). The results of MTT assays showed the high killing effect of anticancer drugs on HCC cells after co-incubating for 48 h (Fig. 3a). When the time was shortened to 24 h, the cell viability increased to more than 70%, and the cell viability displayed no significant change at low drug concentrations (Fig. 3b). LM3 cells showed much lower sensitivity to all drugs than HepG2 and Huh7 cells when treated with the same concentration of sorafenib, DOX and cisplatin. Particularly, the cell viability of LM3 cells showed an increasing tendency after being treated with sorafenib for 24 h when the drug concentration ranged from 0.31 to 2.5 μmol L^{-1}.

In the ATP assays, the cell viability of all HCC cells decreased to less than 40% after 48 h of treatment with the highest concentration of drugs. In contrast, when the time was shortened to 24 h, the viability of all cell lines increased first and then decreased with the increase of drug concentration, especially in the groups of LM3-sorafenib and LM3-CDDP (Fig. S8). The phenomenon that ATP increased first and then decreased while MTT decreased continuously has been reported [34], which may be related to the enhanced glycolysis in cells after stimulated by low concentrations of drugs. Therefore, MTT or ATP assay for drug susceptibility test of the tumor cell to anticancer may result in a different outcome, and the information of cells after drug treatment is not sufficient.

3.3. Fatty acids that associated with the degree of drug response in HCC cells

It has been reported that the peak ratio of different fatty acids might be related to tumor lesions. For example, the ratio value of docosahexaenoic acid (C22:6)/arachidonic acid (C20:4) was observed to decrease in tumor tissues [35,36]. Fatty acids can be sensitively detected owing to their high ionization efficiency. In the present work, the peak intensity of twenty kinds of fatty acids including C16:0, C16:1, C18:0, C18:1, C20:4, C20:5 and C22:6 was measured. The result showed that their distribution in the three HCC cell lines was significantly different (Fig. S5a). The four most abundant fatty acids which constitute more than 80% of total fatty acids were C16:0 (palmitic acid), C18:0 (stearic acid), C16:1 and C18:1. In the present work, we found that the relative ratio values (*Rr*) of C16:1/C16:0 and C18:1/C18:0 changed along with the increase of drug concentration. The "*Rr*" can be calculated by the following equation:

$$Rr(\text{lipid } 1 / \text{ lipid } 2) = \frac{(I_{n-lipid\ 1} / I_{n-lipid\ 2})}{(I_{0-lipid\ 1} / I_{0-lipid\ 2})}$$

Here "I_n" represents the intensity of the corresponding lipid, and the subscript "*n*" corresponds to the concentration of the drug used in the cell samples. "I_0" represents the peak intensity of the corresponding lipid without drug treatment.

As shown in Fig. 4a–f, *Rr*(C16:1/C16:0) and *Rr*(C18:1/C18:0) decreased in almost all drug-treated HCC cells. Taking the group of Hep G2-sorafenib as an example, the relative intensity of C16:1 to C16:0 and C18:1 to C18:0 in the MS spectra decreased significantly with the increase of drug concentration (Fig. 4g and h). However, the ratio values in the groups of LM3-sorafenib and LM3-CDDP slightly fluctuated in an upward trend as the drug concentration increased (Fig. 4a, c, d and f). Although their ratio value did not always show a strong correlation with the drug concentration, a clear relationship between the ratio value and cell viability was observed in all types of cells (Fig. 5a and b). The linear correlations between the ratio values and cell viability in all cell groups were observed with person correlation coefficients (r) of 0.85 and 0.52, respectively. Usually, $r > 0.4$ or $r < -0.4$ indicates a statistically significant correlation. Fig. 5c also shows the high correlation coefficients ($r > 0.7$) between *Rr*(C16:1/C16:0), *Rr*(C18:1/C18:0) and cell viability of each HCC cell line after incubating with different drugs, and their correlation did not depend on cell subtypes or drug types.

The *de novo* fatty acid synthesis pathway is the primary source of endogenous fatty acids in tumor cells. Palmitic acid (C16:0) is the direct product of FA *de novo* synthesis and can be catalyzed to stearic acid (C18:0) by elongase of very long-chain fatty acid 6 (ELOVL6). Palmitic acid was reported to alter lipid metabolism by multiple mechanisms [37] and could be an alternative parameter to indicate the cell proliferation of HCC cells [38]. Palmitoleic acid (C16:1n-7) and oleic acid (C18:1n-9) are the most abundant monounsaturated fatty acids in cells, both of them are the desaturation products of C16:0 and C18:0 catalyzed by stearoyl-CoA desaturase 1(SCD1). The synthesis pathway of C16:0, C18:0, C16:1 and C18:1 was shown in Fig. 5d. SCD1 is often overexpressed in cancer cells and is regarded as a potential target of anticancer drugs [39–41]. The ratio values of C16:1/C16:0 and C18:1/C18:0 could be the index of SCD1 activity. It has been reported that C16:1/C16:0 and C18:1/C18:0 increased in human prostate tumors and significantly decreased in growth-inhibited tumors. A study on the target mechanism of sorafenib to HCC cells also demonstrated that the cellular steady-state levels of C16:1 and C18:1 decreased by sorafenib treatment in a time-dependent manner [42]. Therefore, the ratio values of C16:1/C16:0 and C18:1/C18:0 may become good indicators of HCC cell viability. We further investigated the expression of SCD1 in the drug-treated Huh7 cells by Western blot experiments, the changing of its expression level was highly in accordance with the changing of *Rr* (C16:1/C16:0) and *Rr*(C18:1/C18:0) in each group (Fig. 5e). In addition, The MS-based approach was more sensitive than the conventional cell viability assay. For example, the cell viability of Hep G2 measured by MTT assay decreased to 90% after incubating with 0.63 μmol L^{-1} sorafenib for 24 h (Fig. 3b), while the ratio values of C16:1/C16:0 and C18:1/C18:0 decreased to 75% and 65% (Fig. 4g and h). After treatment with the 2.5 μmol L^{-1} sorafenib for 24 h, the cell viability of Hep G2

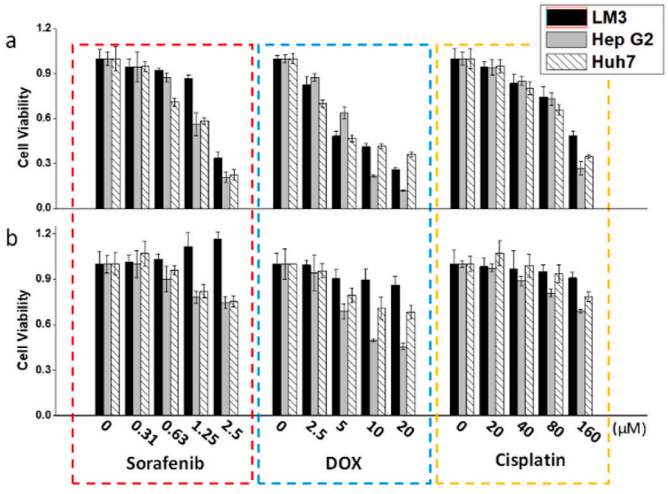

Fig. 3. Cell viability of LM3, Hep G2 and Huh7 cells after treatment with different concentrations of sorafenib, DOX or cisplatin for (a) 48 h and (b) 24 h. All were measured by MTT assay.

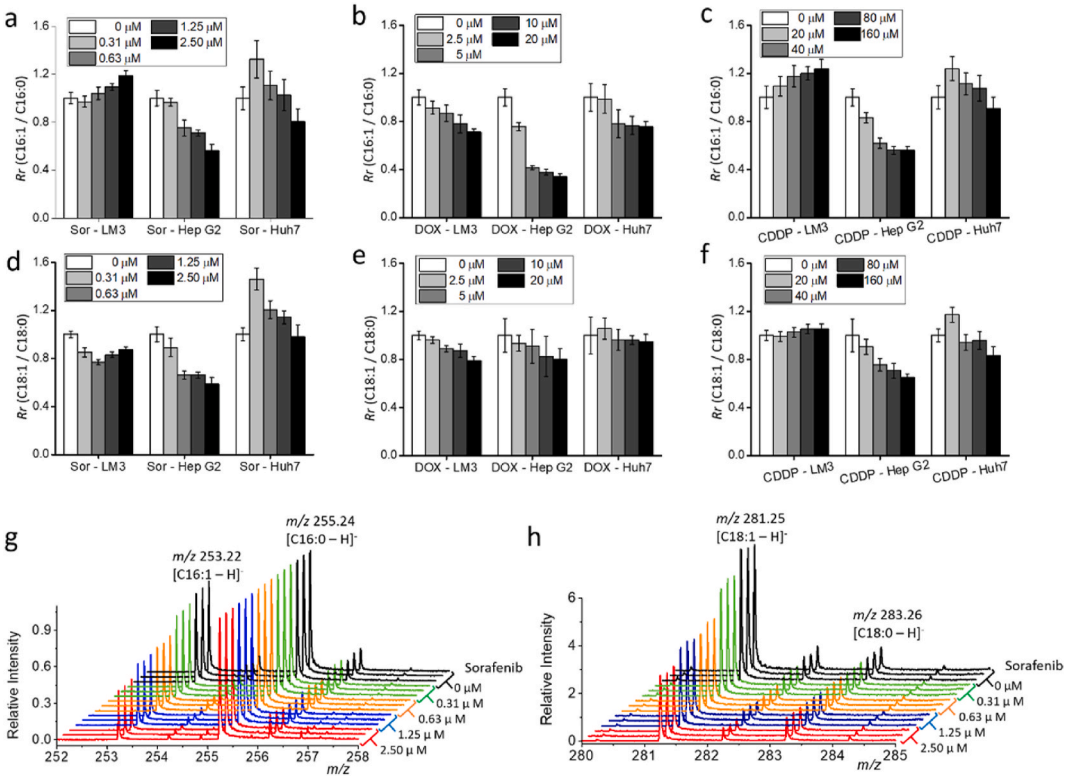

Fig. 4. The change of (a–c) *Rr*(C16:1/C16:0) and (d–f) *Rr*(C18:1/C18:0) in LM3, Hep G2 and Huh7 cells after incubating with a series concentration of sorafenib, DOX and CDDP for 24 h. Mass spectra of (g) C16:0, C16:1, (h) C18:0 and C18:1 in Hep G2 cells that had been treated with different concentrations of sorafenib for 24 h. The intensity of C16:1 and C18:1 were normalized by the intensity of C16:0 and C18:0, respectively. μM: μmol L^{-1}.

measured by MTT assay decreased to 74% (Fig. 3b), while the ratio values of C16:1/C16:0 and C18:1/C18:0 decreased to 56% and 58% (Fig. 4g and h). Clearly, compared with the MTT assay, the change of C16:1/C16:0 and C18:1/C18:0 ratios could be a sensitive indicator to evaluate cell apoptosis caused by anticancer drugs for different HCC cells.

As the ratios of C16:1/C16:0 and C18:1/C18:0 changed with the effect of anticancer drugs on HCC cells, we invested the correlation between C16:1/C16:0, C18:1/C18:0 and phospholipids who containing same polar heads and different fatty acid chains of C16:1, C16:0, C18:1 and C18:0 (Fig. S9). For instance, PE 34:2 and PE 34:1 were identified as PE(16:1/18:1) and PE(16:0/18:1), and the change of PE 34:2/PE 34:1 ratio value was positively correlated to the ratio of C16:1/C16:0. The same tendency also occurred between PA (18:1/18:1)/PA (18:0/18:1) and C18:1/C18:0. However, the relationship between C16:1/C16:0, C18:1/C18:0 and phospholipid pairs were not always positively correlated (Fig. S9) because the expression of phospholipids involves complex biosynthesis and metabolic pathways.

3.4. Feature phospholipid pairs that were related to the drug response of specific cell lines or drug types

The heterogeneity of HCC cells is an obstacle to efficient chemotherapy for their diverse response to anticancer drugs. Previous studies have demonstrated variant protein expression responses of different HCC cell lines to sorafenib and DOX treatment [43,44]. In the present work, LM3 cells showed resistance to sorafenib and CDDP compared to Hep G2 cells and Huh7 cells while all HCC cells were sensitive to DOX. This result indicated that heterogeneous HCC cells do have different sensitivities to the same drug, and their resistance to drugs may come from different regulatory mechanisms that may result in corresponding changes of characteristic lipid molecules for different cell lines. However, the different drug response behavior cannot be revealed by the *Rr* value of fatty acids C16:1/C16:0 and C18:1/C18:0, which only act as a comprehensive indicator for HCC viability. Therefore, lipid indicators for drug susceptibility tests on different types of HCC cell lines were further investigated.

The distribution of phospholipids detected in the three types of HCC cells was slightly different (Fig. S5b). In this study, we regarded adjacent lipid peaks that sharing similar structures with only difference in unsaturation degree as internal standards for each other. Actually, several pairs of adjacent phospholipids whose *Rr* value related to the differential response of each HCC cell line to drugs were found. The ratio of *Rr*(PA 34:2/PA 34:1) showed good linearity to the cell viability of LM3 in all drug-treated groups (Fig. 6a), which was the same as the behavior of *Rr*(PC 36:4/PC 36:3) to Hep G2 cells (Fig. 6b). The *Rr*(PE 37:6/PE 37:4) was found to be a good index to indicate the response of LM3, Hep G2 and Huh7 cells to CDDP because it showed good linearity to cell viability (Fig. 6c).

These adjacent phospholipids pairs relating to a specific subtype of cells or specific drug might provide new guidance for the evaluation of drug efficacy for HCC patients with specific tumor subtypes in the clinic. The correlation among the identified lipids of each HCC cell after treated with drugs was analyzed by a clustered correlation matrix. Several clusters in the matrix were visualized as red squares with high correlation, implying phospholipids in the same cluster might participate in the same metabolic pathways responding to the drug treatment (Fig. 7a, d, g). For each HCC cell line, the molecular types of phospholipids in these highly correlated clusters were significantly different. For example, in clusters of LM3 cells, several PC and PE molecules were highly correlated (Fig. 7b and c). The main species of highly correlated lipids in Huh7 cells were PI, PS and PE (Fig. 7e and f), and mainly PE molecules were highly correlated in Hep G2 cells (Fig. 7h). These results indicated that different lipids could reflect the different drug responses of these three HCC cell lines.

Additionally, the cell membrane fluidity is influenced by the

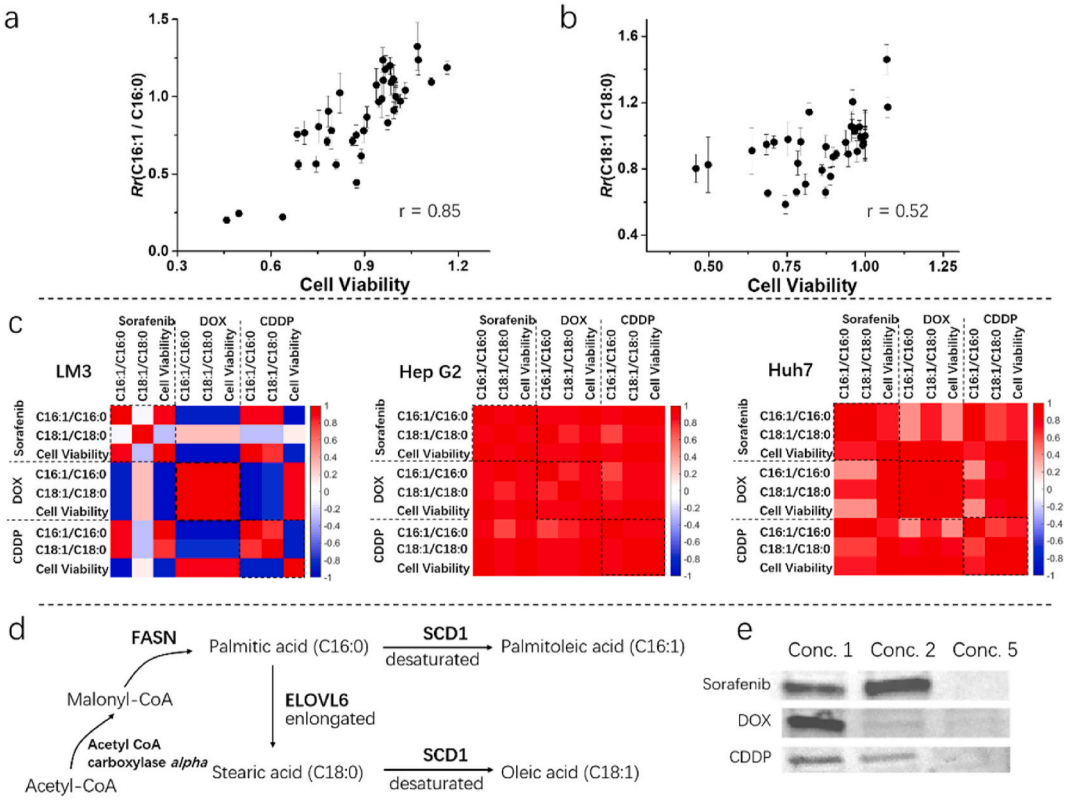

Fig. 5. Correspondences between cell viability and the relative ratio values of (a) *Rr*(C16:1/C16:0), (b) *Rr*(C18:1/C18:0) in LM3, Hep G2 and Huh7 cells that had incubated with a series concentration of with sorafenib, DOX and CDDP for 24 h. (c) Spearman correlation coefficients matrix of *Rr*(C16:1/C16:0), *Rr*(C18:1/C18:0) and cell viability for LM3, Hep G2 and Huh7 cells that had been treated with series concentration of sorafenib, DOX and CDDP for 24 h. (d) The biosynthesis pathways of C16:0, C16:1, C18:0 and C18:1. (e) Expression profile of SCD1 in the drug-treated Huh7 cells. Abbreviation: CoA, coenzyme A; FAS, FA synthase; SCD1, stearoyl-CoA desaturase 1; SFA, saturated FA; ELOVL6, elongase of very long chain fatty acid 6.

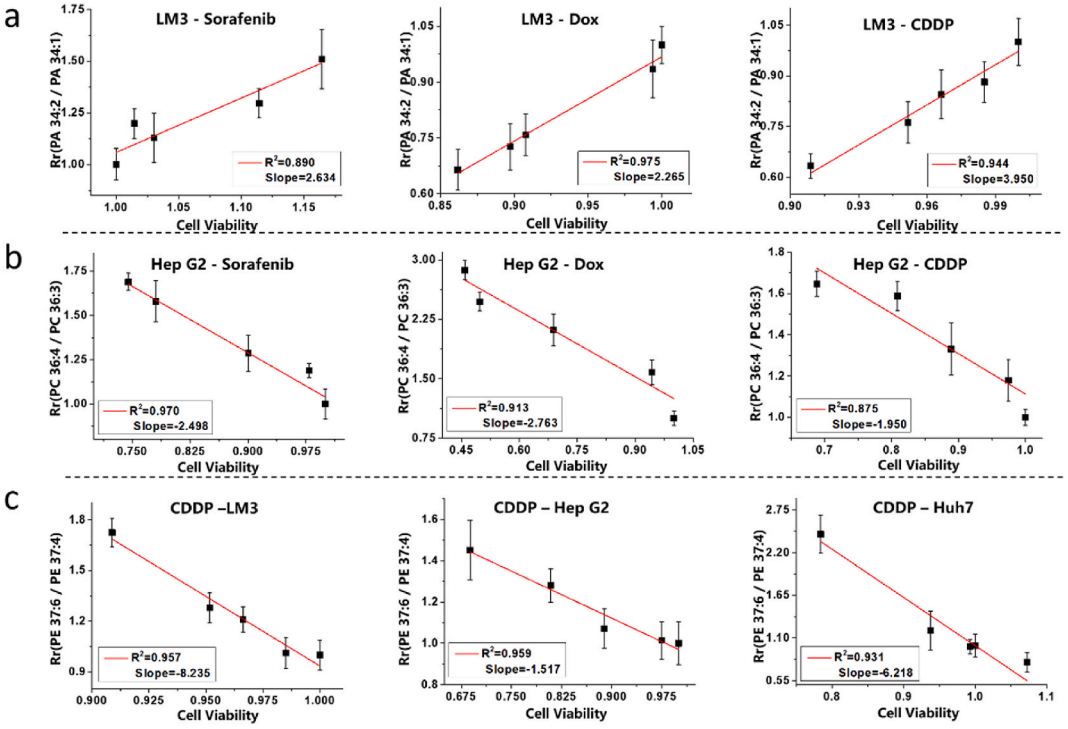

Fig. 6. Characteristic phospholipid pairs whose ratio values showed good linearity to cell viability of (a) drug-treated LM3 cells, (b) drug-treated Hep G2 cells and (c) all cells that had been treated with CDDP. *Rr*: relative ratio value.

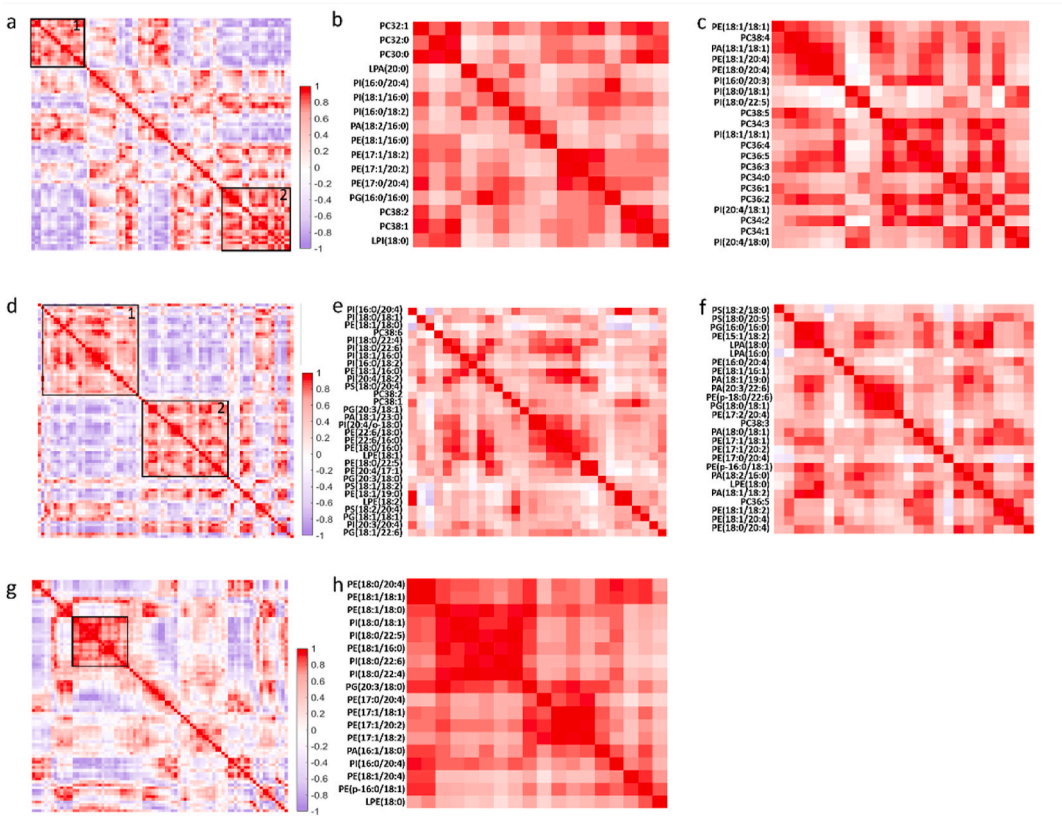

Fig. 7. The clustered correlation matrix of the identified phospholipids of (a–c) drug-treated LM3 cells, (d–f) drug-treated Huh7 cells and (g–h) Hep G2 cells. (b–c) are the magnification of the squared clusters 1 and 2 in (a), respectively. (e–f) are the magnification of the squared clusters 1 and 2 in (d), respectively. (h) is the magnification of the squared cluster in (g).

proportion of membrane phospholipids with constituents of poly-unsaturated fatty acids (PUFAs, degree of unsaturation >1), and the increase of polyunsaturated phospholipids will upregulate the fluidity of the cell membrane [45]. In this work, we found the increase of poly-unsaturated lipids in all drug-treated HCC cells (Fig. S10). Although anticancer agents could induce apoptosis of tumor cells through alternating membrane fluidity [46], there is no sufficient evidence for the relationship between the drug-induced increase in cell membrane fluidity and cell apoptosis. The increase or decrease of membrane fluidity in cisplatin or DOX-resistant tumor cells has been reported [47,48]. The specific relationship between cell membrane fluidity and drug sensitivity/resistance of tumor cells remains to be studied in depth.

4. Conclusions

In the present work, we proposed a high-throughput MS method to evaluate the drug response of heterogeneous HCC cells to different types of anticancer drugs. The use of a high-throughput Si-NALDI target facilitated the rapid detection of fatty acids and phospholipids of HCC cells with high reproducibility. The results demonstrated that HCC cells had metabolic responses to types of drug treatment, and the paired phospholipids might be a potential indicator for precise drug screening for patients with specific tumor subtypes. The MS-based approach is multi-functional since it can simultaneously identify HCC cell subtypes, evaluate cell cytotoxicity and discover drug-sensitive lipids involved in metabolic pathways. Owing to its advantages of high-throughput, simple procedures and good stability, this platform could be a potential candidate for precise tumor chemosensitivity assay on the molecular level, and has the potential to investigate the toxicity mechanism of anticancer drugs to heterogeneous cancer cells that may promote the development of individualized tumor treatment.

Funding

This research was funded by the National Natural Science Foundation of China (NSFC), grant number 21874118, 21575127.

Declaration of competing interest

The authors declare that they have no known competing financial interests or personal relationships that could have appeared to influence the work reported in this paper.

Appendix A. Supplementary data

Supplementary data to this article can be found online at https://doi.org/10.1016/j.talanta.2021.122817.

Credit author statement

Tao Wang: Formal analysis, Methodology, Software, Writing – original draft. **Xingyue Liu:** Validation, Visualization. **Xuetong Qu:** Investigation, Supervision. **Yuexin Li:** Investigation, Supervision. **Xiao Liang:** Conceptualization, Resources. **Jianmin Wu:** Funding acquisition, Data curation, Writing – review & editing. All authors have read and agreed to the published version of the manuscript.

References

[1] A. Forner, M. Reig, J. Bruix, Hepatocellular carcinoma, Lancet 391 (2018) 1301–1314.

[2] L.C. Lu, C.H. Hsu, C. Hsu, A.L. Cheng, Tumor heterogeneity in hepatocellular carcinoma: facing the challenges, Liv. Canc. 5 (2016) 128–138.

[3] D.C. Lin, A. Mayakonda, H.Q. Dinh, P. Huang, L. Lin, X. Liu, L.W. Ding, J. Wang, B. P. Berman, E.W. Song, D. Yin, H.P. Koeffler, Genomic and epigenomic heterogeneity of hepatocellular carcinoma, Canc. Res. 77 (2017) 2255–2265.

[4] K.S. Jeng, C.F. Chang, W.J. Jeng, I.S. Sheen, C.J. Jeng, Heterogeneity of hepatocellular carcinoma contributes to cancer progression, Crit. Rev. Oncol.-Hematol. 94 (2015) 337–347.

[5] Z. Guo, L.Q. Li, J.H. Jiang, C. Ou, L.X. Zeng, B.D. Xiang, Cancer stem cell markers correlate with early recurrence and survival in hepatocellular carcinoma, World J. Gastroenterol. 20 (2014) 2098–2106.

[6] A. Fujimoto, M. Furuta, Y. Shiraishi, K. Gotoh, Y. Kawakami, K. Arihiro, T. Nakamura, M. Ueno, S. Ariizumi, H.H. Nguyen, D. Shigemizu, T. Abe, K. A. Boroevich, K. Nakano, A. Sasaki, R. Kitada, K. Maejima, Y. Yamamoto, H. Tanaka, T. Shibuya, T. Shibata, H. Ojima, K. Shimada, S. Hayami, Y. Shigekawa, H. Aikata, H. Ohdan, S. Marubashi, T. Yamada, M. Kubo, S. Hirano, O. Ishikawa, M. Yamamoto, H. Yamaue, K. Chayama, S. Miyano, T. Tsunoda, H. Nakagawa, Whole-genome mutational landscape of liver cancers displaying biliary phenotype reveals hepatitis impact and molecular diversity, Nat. Commun. 6 (2015) 6120.

[7] I.C. Hsu, R.A. Metcalf, T. Sun, J.A. Welsh, N.J. Wang, C.C. Harris, Mutational hotspot in the p53 gene in human hepatocellular carcinomas, Nature 350 (1991) 427–428.

[8] J.C. Nault, J. Calderaro, L. Di Tommaso, C. Balabaud, E.S. Zafrani, P. Bioulac-Sage, M. Roncalli, J. Zucman-Rossi, Telomerase reverse transcriptase promoter mutation is an early somatic genetic alteration in the transformation of premalignant nodules in hepatocellular carcinoma on cirrhosis, Hepatology 60 (2014) 1983–1992.

[9] Z. von Marschall, T. Cramer, M. Hocker, G. Finkenzeller, B. Wiedenmann, S. Rosewicz, Dual mechanism of vascular endothelial growth factor upregulation by hypoxia in human hepatocellular carcinoma, Gut 48 (2001) 87–96.

[10] A.B. Siegel, E.I. Cohen, A. Ocean, D. Lehrer, A. Goldenberg, J.J. Knox, H. Chen, S. Clark-Garvey, A. Weinberg, J. Mandeli, P. Christos, M. Mazumdar, E. Popa, R. S. Brown Jr., S. Rafii, J.D. Schwartz, Phase II trial evaluating the clinical and biologic effects of bevacizumab in unresectable hepatocellular carcinoma, J. Clin. Oncol. 26 (2008) 2992–2998.

[11] S. Whittaker, R. Marais, A.X. Zhu, The role of signaling pathways in the development and treatment of hepatocellular carcinoma, Oncogene 29 (2010) 4989–5005.

[12] C.H. Johnson, J. Ivanisevic, G. Siuzdak, Metabolomics: beyond biomarkers and towards mechanisms, Nat. Rev. Mol. Cell Biol. 17 (2016) 451–459.

[13] R.D. Blumenthal, D.M. Goldenberg, Methods and goals for the use of in vitro and in vivo chemosensitivity testing, Mol. Biotechnol. 35 (2007) 185–197.

[14] T. Mosmann, Rapid colorimetric assay for cellular growth and survival: application to proliferation and cytotoxicity assays, J. Immunol. Methods 65 (1983) 55–63.

[15] S.P.M. Crouch, R. Kozlowski, K.J. Slater, J. Fletcher, The use of Atp bioluminescence as a measure of cell-proliferation and cytotoxicity, J. Immunol. Methods 160 (1993) 81–88.

[16] V.N. Sumantran, Cellular chemosensitivity assays: an overview, Methods Mol. Biol. 731 (2011) 219–236.

[17] Ph D. Hans-Jürgen Rode, Doris Eisel, Roche Applied Science: Apoptosis, Cell Death, and Cell Proliferation Manual, fourth ed., 2008. Indianapolis, United States.

[18] R. Kim, M. Emi, K. Tanabe, Y. Uchida, K. Arihiro, The role of apoptotic or nonapoptotic cell death in determining cellular response to anticancer treatment, Eur. J. Surg. Oncol. 32 (2006) 269–277.

[19] X.M. Chen, F.J. Wo, J. Chen, J. Tan, T. Wang, X. Liang, J.M. Wu, Ratiometric mass spectrometry for cell identification and quantitation using intracellular "Dual-Biomarkers, Sci. Rep. 7 (2017).

[20] T. Wang, X. Chen, C. Luan, J. Wu, High throughput lipid profiling for subtype classification of hepatocellular carcinoma cell lines and tumor tissues, Anal. Chim. Acta 1107 (2020) 92–100.

[21] X. Wang, R. Hui, Y. Chen, W. Wang, Y. Chen, X. Gong, J. Jin, Discovery of novel doxorubicin metabolites in MCF7 doxorubicin-resistant cells, Front. Pharmacol. 10 (2019) 1434.

[22] M.Y. Lee, A. Yeon, M. Shahid, E. Cho, V. Sairam, R. Figlin, K.H. Kim, J. Kim, Reprogrammed lipid metabolism in bladder cancer with cisplatin resistance, Oncotarget 9 (2018) 13231–13243.

[23] V. Behrends, G.F. Giskeodegard, N. Bravo-Santano, M. Letek, H.C. Keun, Acetaminophen cytotoxicity in HepG2 cells is associated with a decoupling of glycolysis from the TCA cycle, loss of NADPH production, and suppression of anabolism, Arch. Toxicol. 93 (2019) 341–353.

[24] E. Berghmans, K. Boonen, E. Maes, I. Mertens, P. Pauwels, G. Baggerman, Implementation of MALDI mass spectrometry imaging in cancer proteomics research: applications and challenges, J. Personalized Med. 10 (2020).

[25] J. Wei, J.M. Buriak, G. Siuzdak, Desorption-ionization mass spectrometry on porous silicon, Nature 399 (1999) 243–246.

[26] J. Sunner, E. Dratz, Y.C. Chen, Graphite surface-assisted laser desorption/ionization time-of-flight mass spectrometry of peptides and proteins from liquid solutions, Anal. Chem. 67 (1995) 4335–4342.

[27] T.R. Northen, O. Yanes, M.T. Northen, D. Marrinucci, W. Uritboonthai, J. Apon, S. L. Golledge, A. Nordstrom, G. Siuzdak, Clathrate nanostructures for mass spectrometry, Nature 449 (2007) 1033–1036.

[28] M.J. Kang, J.C. Pyun, J.C. Lee, Y.J. Choi, J.H. Park, J.G. Park, J.G. Lee, H.J. Choi, Nanowire-assisted laser desorption and ionization mass spectrometry for quantitative analysis of small molecules, Rapid Commun. Mass Spectrom. 19 (2005) 3166–3170.

[29] B.N. Walker, J.A. Stolee, D.L. Pickel, S.T. Retterer, A. Vertes, Tailored silicon nanopost arrays for resonant nanophotonic ion production, J. Phys. Chem. C 114 (2010) 4835–4840.

[30] G. Schlosser, G. Pocsfalvi, E. Huszar, A. Malorni, F. Hudecz, MALDI-TOF mass spectrometry of a combinatorial peptide library: effect of matrix composition on signal suppression, J. Mass Spectrom. 40 (2005) 1590–1594.

[31] J. Folch, M. Lees, G.H. Sloane Stanley, A simple method for the isolation and purification of total lipides from animal tissues, J. Biol. Chem. 226 (1957) 497–509.

[32] X. Chen, J. Gao, T. Wang, X. Jiang, J. Chen, X. Liang, J. Wu, Hepatocarcinoma discrimination by ratiometric lipid profiles using tip-contact sampling/ionization mass spectrometry, Anal. Chem. 91 (2019) 10376–10380.

[33] X. Chen, T. Wang, L. Lin, F. Wo, Y. Liu, X. Liang, H. Ye, J. Wu, Tip-enhanced photoinduced electron transfer and ionization on vertical silicon nanowires, ACS Appl. Mater. Interfaces 10 (2018) 14389–14398.

[34] Y. Liu, X.D. Song, W. Liu, T.Y. Zhang, J. Zuo, Glucose deprivation induces mitochondrial dysfunction and oxidative stress in PC12 cell line, J. Cell Mol. Med. 7 (2003) 49–56.

[35] J.J. Zhang, L.J. Zhang, X.X. Ye, L.Y. Chen, L.T. Zhang, Y.H. Gao, J.X. Kang, C. Cai, Characteristics of fatty acid distribution is associated with colorectal cancer prognosis, Prostag. Leukotr. Ess. 88 (2013) 355–360.

[36] J.F. Qiu, K.L. Zhang, X.J. Zhang, Y.J. Hu, P. Li, C.Z. Shang, J.B. Wan, Abnormalities in plasma phospholipid fatty acid profiles of patients with hepatocellular carcinoma, Lipids 50 (2015) 977–985.

[37] C. Garcia-Ruiz, J.M. Mato, D. Vance, N. Kaplowitz, J.C. Fernandez-Checa, Acid sphingomyelinase-ceramide system in steatohepatitis: a novel target regulating multiple pathways, J. Hepatol. 62 (2015) 219–233.

[38] W.Q. Xu, X. Zhang, J.L. Wu, L. Fu, K. Liu, D.B. Liu, G.G. Chen, P.B.S. Lai, N. Wong, J. Yu, O-GlcNAc transferase promotes fatty liver-associated liver cancer through inducing palmitic acid and activating endoplasmic reticulum stress, J. Hepatol. 67 (2017) 310–320.

[39] A. Beckers, S. Organe, L. Timmermans, K. Scheys, A. Peeters, K. Brusselmans, G. Verhoeven, J.V. Swinnen, Chemical inhibition of acetyl-CoA carboxylase induces growth arrest and cytotoxicity selectively in cancer cells, Canc. Res. 67 (2007) 8180–8187.

[40] B. Peck, Z.T. Schug, Q. Zhang, B. Dankworth, D.T. Jones, E. Smethurst, R. Patel, S. Mason, M. Jiang, R. Saunders, M. Howell, R. Mitter, B. Spencer-Dene, G. Stamp, L. McGarry, D. James, E. Shanks, E.O. Aboagye, S.E. Critchlow, H.Y. Leung, A. L. Harris, M.J.O. Wakelam, E. Gottlieb, A. Schulze, Inhibition of fatty acid desaturation is detrimental to cancer cell survival in metabolically compromised environments, Canc. Metabol. 4 (2016) 6.

[41] G. Lucarelli, M. Ferro, D. Loizzo, C. Bianchi, D. Terracciano, F. Cantiello, L.N. Bell, S. Battaglia, C. Porta, A. Gernone, R.A. Perego, E. Maiorano, O. Cobelli, G. Castellano, L. Vincenti, P. Ditonno, M. Battaglia, Integration of lipidomics and transcriptomics reveals reprogramming of the lipid metabolism and composition in clear cell renal cell carcinoma, Metabolites 10 (2020).

[42] G. Liu, S. Kuang, R.B. Cao, J. Wang, Q.C. Peng, C.M. Sun, Sorafenib kills liver cancer cells by disrupting SCD1-mediated synthesis of monounsaturated fatty acids via the ATP-AMPK-mTOR-SREBP1 signaling pathway, Faseb. J. 33 (2019) 10089–10103.

[43] Y. Zhu, J.G. Xu, W. Hu, F. Wang, Y. Zhou, W. Xu, W. Gong, L.C. Shao, TFAM depletion overcomes hepatocellular carcinoma resistance to doxorubicin and sorafenib through AMPK activation and mitochondrial dysfunction, Gene (2020) 753.

[44] F.Q. Wu, T. Fang, L.X. Yu, G.S. Lv, H.W. Lv, D. Liang, T. Li, C.Z. Wang, Y.X. Tan, J. Ding, Y. Chen, L. Tang, L.N. Guo, S.H. Tang, W. Yang, H.Y. Wang, ADRB2 signaling promotes HCC progression and sorafenib resistance by inhibiting autophagic degradation of HIF1 alpha, J. Hepatol. 65 (2016) 314–324.

[45] J.C. Holthuis, A.K. Menon, Lipid landscapes and pipelines in membrane homeostasis, Nature 510 (2014) 48–57.

[46] S. Baritaki, S. Apostolakis, P. Kanellou, M.T. Dimanche-Boitrel, D.A. Spandidos, B. Bonavida, Reversal of tumor resistance to apoptotic stimuli by alteration of membrane fluidity: therapeutic implications, Adv. Canc. Res. 98 (2007) 149–190.

[47] X.J. Liang, J.J. Yin, J.W. Zhou, P.C. Wang, B. Taylor, C. Cardarelli, M. Kozar, R. Forte, A. Aszalos, M.M. Gottesman, Changes in biophysical parameters of plasma membranes influence cisplatin resistance of sensitive and resistant epidermal carcinoma cells, Exp. Cell Res. 293 (2004) 283–291.

[48] L. Zong, Z. Pi, S. Liu, J. Xing, Z. Liu, F. Song, Liquid extraction surface analysis nanospray electrospray ionization based lipidomics for in situ analysis of tumor cells with multidrug resistance, Rapid Commun. Mass Spectrom. 32 (2018) 1683–1692.